Materials Advances

ROYAL SOCIETY OF CHEMISTRY

PAPER

View Article Online
View Journal | View Issue

Cite this: *Mater. Adv.*, 2022, 3, 4870

A hydrophobic imidazolium cationic framework for selective adsorption of TcO_4^-/ReO_4^- from aqueous solutions†

Xupeng Zhi,[a] Xiaomin Li,[a] Fangfei Dong,[a] Yiwei Huang,[a] Suliang Yang,*[b] Taihong Yan*[b] and Yinglin Shen *[a]

Traditional anion exchangers for TcO_4^- usually have low selectivity and adsorption capacity due to the lack of functional groups that interact strongly with TcO_4^-. Here, we report a three-dimensional imidazolium network IMI-P that exhibits high adsorption capacity, fast kinetics, and outstanding selectivity for ReO_4^-/TcO_4^- at pH 2–13. It can remove 90% of ReO_4^- in 30 s and 99% ReO_4^- in 10 min, which is significantly faster than most commercial materials. Besides, the maximum sorption capacity of IMI-P (792 mg ReO_4^-/g) is also higher than that of most commercial materials. IMI-P shows good TcO_4^- removal efficiencies for simulated wastewater, which can reach 91.5% and 98.4% at the solid–liquid ratio of 10 g L^{-1} and 50 g L^{-1}, respectively. Compared with other Tc-adsorption polymers, IMI-P with a larger particle size (10–30 μm) is more suitable for column chromatography separation. Therefore, IMI-P has important application potential in wastewater treatment in the nuclear industry. The adsorption mechanism of IMI-P and the interaction mode with ReO_4^- were also studied by IR, EDS, and XPS.

Received 26th February 2022,
Accepted 18th April 2022

DOI: 10.1039/d2ma00220e

rsc.li/materials-advances

Introduction

Nuclear energy is gaining more public attention due to increased energy demand and limited reserves of fossil fuel.[1] However, the key to the development of nuclear energy is to systematically handle the radioactive waste generated by spent fuel and avoid nuclear accidents.[2,3] Large amounts of radionuclides are created from the fission of ^{235}U and ^{239}Pu, and among them, ^{99}Tc is one of the most problematic and notorious nuclides. The long half-life (2.1×10^5 years) and high fission yield (6.1%) of this β-emitting nuclide determine that it should be immobilized and stored in deep geological repositories.[4,5] However, hepta-valent Tc compounds such as Tc_2O_7 have high volatility at the vitrification temperature and will leach with off-gas.[6,7] TcO_4^- is difficult to adsorb in the natural environment, is highly soluble in water, is highly mobile underground, and is chemically stable.[8,9] Therefore, sequestering TcO_4^- from waste liquid is meaningful for optimizing the reprocessing and preventing environmental pollution.[10]

Many methods are proposed that aim at removing Tc from waste water, such as photoreduction and chemical reduction, coprecipitation, solvent extraction, and ion exchange.[11–14] Due to its low cost and easy implementation, ion exchange has become one of the most commonly used methods and myriads of ion exchange materials have been designed to remove Tc. Inorganic ion-exchange materials have the advantages of easy synthesis and high resistance of radiation and chemical corrosion, attracting chemists to design a variety of such materials, such as LDHs, LRHs, and super-tetrahedral cationic framework NDTB-1, while a low adsorption capacity limits the application of these materials.[15–17] Organic and inorganic grafting materials have uncontrolled grafting rates and low capacity.[18] Ionic metal–organic materials (iMOFs), with the advantages of predictability of structure and controllability of pore size were used for adsorption of TcO_4^- from aqueous solutions, while the low stability limited their applications.[19–23] Organic polymer materials have the advantages of tunable structure due to the wide variety of monomers, and easy to introduce different cationic active sites. Many such materials were designed and synthesized for the adsorption of technetium, some of which were synthesized by a simple quaternization reaction.[24–29] Cationic active groups in these materials include quaternary ammonium salts, imidazolium, pyridine and quaternary phosphonium,[27,30–32] of which imidazolium has the best affinity for ReO_4^-/TcO_4^-. For example, SCU-CPN-1, mPOP-1 and PC2vimer contain abundant imidazolium active sites with higher capacity and selectivity for TcO_4^-/ReO_4^- than other materials.[24,27,33] The reason is that imidazolium cations not only have Coulomb

[a] School of Nuclear Science and Technology, Lanzhou university, 730099, Lanzhou, China. E-mail: shenyl@lzu.edu.cn
[b] Radiochemistry Department, China Institute of Atomic Energy, Beijing, 102413, China

† Electronic supplementary information (ESI) available. See DOI: https://doi.org/10.1039/d2ma00220e

electrostatic interactions with anions, but also have p–π interactions with ReO_4^-/TcO_4^-.[27]

Here, an imidazolium cationic polymer, IMI-P, was synthesized *via* an easy one-pot reaction of nucleophilic substitution between tetrahedral imidazolylphenylmethanes and polyhalogenated benzenes, the backbone of which contains multiple benzene rings that will provide considerable hydrophobicity and radiation resistance. A similar material with the same design idea but different synthesis processes, CPN-tpm-Cl, shows different microscopic morphology and characteristics compared with IMI-P. IMI-P exhibits a lower degree of imidazole quaternization, but a higher selectivity to ReO_4^-/TcO_4^- compared with CPN-tpm-Cl.[34] Following the Hofmeister bias, soft ReO_4^-/TcO_4^- with low charge density has better affinity for the hydrophobic material IMI-P. The structure of the material is an important factor affecting the adsorption kinetics. The use of tetrahedral imidazolylphenylmethane as the starting material in the polymerization reaction ensures the formation of a three-dimensional structure similar to PPN-6, which favors adsorption kinetics.[35] A bottom-up synthesis strategy was adopted to ensure a high density of exchange sites for the material, which is beneficial to improve the adsorption capacity.[36] In addition, IMI-P has a larger particle diameter (10–30 μm) compared to the cationic polymer network SCU-CPN-1 (2 μm),[27] which facilitates practical applications. The adsorption performances in different acidic and alkaline aqueous solutions and simulated nuclear wastewater were also investigated.

Experimental section

Chemicals and reagents

Safety Notes. ^{99}Tc is a β-emitter (E_{max} = 294 keV, $t_{1/2} = 2 \times 10^5$ years). All operations were carried out in radiochemical laboratories equipped for handling this isotope. Because of the radioactivity of TcO_4^-, ReO_4^- was used as a non-radioactive analogue of $^{99}TcO_4^-$ in some experiments.

All reagents were obtained from Aldrich and used as received. ^{99}Tc (as NH_4TcO_4) was obtained from China Institute of Atomic Energy stocks. Rhenium was obtained as NH_4ReO_4 from Sigma-Aldrich. ReO_4^- solutions were prepared by dissolving a certain amount of NH_4ReO_4 in distilled water. Tetrakis[4-(1*H*-imidazol-1-yl)-phenyl]methane and 1,4-bis(chloromethyl)benzene were provided by Nanjing Mole Medical Science & Technology Co., Ltd and Shanghai Aladdin Biochemical Technology Co., Ltd, respectively.

IMI-P synthesis

A flask was charged with tetrakis[4-(1*H*-imidazol-1-yl)-phenyl]-methane (2.0 g, 3.42 mmol), 1,4-bis(chloromethyl)benzene-(1.20 g, 6.84 mmol), and anhydrous acetonitrile (30 mL). The mixture was heated to 80 °C and stirred for 72 hours to afford a white solid. The white solid was filtered and washed with acetonitrile and ethanol three times, respectively, and dried at 60 °C, then milled by mortar to afford 2080 mg of IMI-P as a white powder.

General procedure

A typical adsorption experiment was conducted as follows: a certain amount of IMI-P was added into a 10 mL centrifuge tube containing ReO_4^-/TcO_4^- solution at room temperature. Upon shaking in the oscillator for a certain time, the supernatant was separated by a 0.22 μm membrane filter, and the content of Re was determined using the inductively coupled plasma optical emission spectrum (ICP-OES), and the Tc content was determined by liquid scintillation counting.

The ReO_4^- loaded IMI-P for characterization was prepared as follows. 50 mg of IMI-P was added into a 50 mL centrifuge tube containing 18.75 mL of ReO_4^- solution (3000 ppm). After shaking for 12 hours, the solid was separated and washed with deionized water, and then dried under 60 °C.

Adsorption kinetic experiments

Every 5 mg of IMI-P was contacted with 5 mL of ReO_4^- aqueous solution (458 ppm) for 0.5 min, 1 min, 3 min, 5 min, 7.5 min, 10 min, 30 min, and 60 min, respectively. The pseudo-first-order (PFO) (1), the pseudo-second-order (PSO) (2), and the mixed-order (MO) (3) model[37] are used to fit the experimental data. Equations of these models can be expressed as follows:

$$\ln(q_e - q_t) = \ln q_e - k_1 t \quad (1)$$

$$\frac{t}{q_t} = \frac{1}{k_2 q_e^2} + \frac{t}{q_e} \quad (2)$$

$$\frac{dq_t}{dt} = k_1(q_e - q_t) + k_2(q_e - q_t)^2 \quad (3)$$

where q_t and q_e are the adsorption amounts (mg g^{-1}) at time t (min) and equilibrium, respectively, and k_1 is the rate constant (min^{-1}) of the pseudo-first-order model, and k_2 is the rate constant (g mg^{-1} min^{-1}) of the pseudo-second-order model.

pH effect study

Re aqueous solutions (200 ppm) with pH 1, 3, 5, 7, 9, 11, and 13 were prepared, respectively, and contacted with IMI-P at a solid-to-liquid ratio of 1 g L^{-1} for 12 h. The pH is adjusted with nitric acid or sodium hydroxide aqueous solution. For the adsorption experiment of 3 M HNO_3, 30 mg of IMI-P was added to 3 mL of ReO_4^- solution (325 ppm) and shaken for 12 hours.

Adsorption isotherm study

The adsorption isotherms were determined by contacting 5 mg of IMI-P with 5 mL of ReO_4^- solutions with initial concentrations of 200, 400, 800, 1000, 1000, 1500, 2000, 2500 and 3000 ppm, respectively. All samples were shaken for 12 hours to achieve sorption equilibrium. All experiments were repeated three times. The experimental data were fitted with a Langmuir model, and the linear equation of the model is expressed as follows,

$$\frac{C_e}{q_e} = \frac{1}{q_m k_l} + \frac{C_e}{q_m} \quad (4)$$

where q_m (mg g^{-1}) is the maximum sorption capacity of perrhenate calculated by the Langmuir model, k_l (L mg^{-1}) is a constant.

Selectivity experiments

Five competitive anions are used for testing, including SO_4^{2-} (15 mM and 150 mM), NO_3^- (15 mM and 150 mM), CO_3^{2-} (15 mM and 150 mM), PO_4^{3-} (15 mM and 150 mM) and Cl^- (150 mM). 5 mg of IMI-P are added to 5 mL of ReO_4^- solution (0.15 mM) containing different concentrations of competing anions and shaken for 12 hours. In order to test the adsorption performance of IMI-P for trace TcO_4^-, a certain amount of sodium sulfate and nitric acid was added to two centrifuge tubes containing 1 mL of TcO_4^- solution (7.31 ppb) and 5 mg of adsorbent, respectively, so that the concentration of SO_4^{2-} was 1000 times that of TcO_4^- and the concentration of HNO_3 is 3 M. Simulated wastewater containing ReO_4^- or TcO_4^- was prepared according to the previous reports[27] respectively and the species of anions are shown in Table 2. ReO_4^- simulated wastewater experiments were conducted at solid–liquid ratios of 1 g L^{-1} and 5 g L^{-1}, and TcO_4^- simulated wastewater experiments were conducted at solid–liquid ratios of 1, 5, 10, 20, 30, 40, and 50 g L^{-1}. The experiments on simulated wastewater were repeated three times.

Desorption test

The ReO_4^- loaded IMI-P for the desorption test was prepared by the following procedures: 100 mg of IMI-P was contacted with 100 mL of ReO_4^- solution (100 ppm) and kept stirring for 12 hours to reach the adsorption equilibrium; the solid was separated and washed with deionized water, then dried at 60 °C. 20 mg of ReO_4^- loaded IMI-P was added into 20 mL of 1 M NaCl or saturated NaCl solutions. After stirring for 12 hours, the supernatant was separated for ICP-OES analysis. For the desorption test at 80 °C, 20 mg of ReO_4^- loaded IMI-P was added into a flask containing 20 mL of 1 M NaCl solution, and kept stirring for 12 hours at 80 °C, and then the mixture was separated for ICP analysis.

Results and discussion

Synthesis and characterization

The one pot quaternization strategy was used to create imidazolium based cationic network IMI-P *via* quaternization between tetrahedral imidazolylphenylmethane and polyhalogenated benzene as depicted in Scheme 1. The reaction of 1,1,2,2-tetrakis(4-(imidazolyl-4-yl)phenyl)ethene (TIPM) with 1,4-bis(chloromethyl)benzene affords a white solid IMI-P. Unlike TIPM, which is highly soluble in ethanol, IMI-P was insoluble in ethanol, water, and other common solvents, indicating its highly cross-linked structure. Scanning electron microscope (Fig. 1a and b) images of IMI-P show the irregular layered morphology with a diameter of 10–30 μm.

The chemical structures and compositions of IMI-P were confirmed by Fourier transform infrared (FTIR) spectra, energy dispersive spectroscopy (EDS) and X-ray photoelectron spectroscopy (XPS). The FT-IR spectrum of IMI-P (Fig. 2) shows the skeleton vibration of the phenyl group at 1608 and 1510 cm^{-1}, the stretching vibration of C–H bonds on the phenyl group at 3110 cm^{-1}, and the bending vibration at 820 cm^{-1}, which also exists in the raw material. A peak at 1483 cm^{-1} in the spectrum of TIPM is assigned to the C═N stretching vibration of imidazole, which disappears after quaternization reaction. New peaks, at 1550 cm^{-1} and 1074 cm^{-1} are assigned to the $C{=}N^+$ stretching vibration of imidazolium,[27] and the peak at 2960 cm^{-1} is assigned to the stretching vibration of methylene.

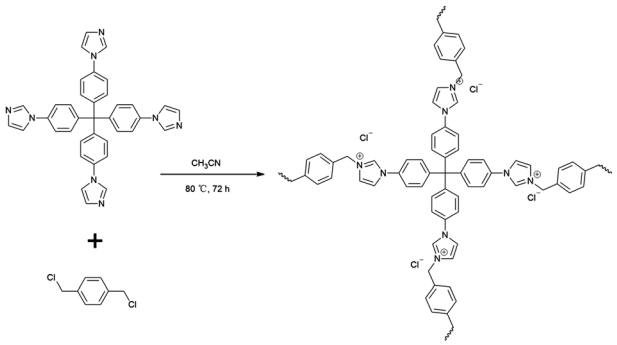

Scheme 1 The synthesis procedure of IMI-P *via* quaternization reaction.

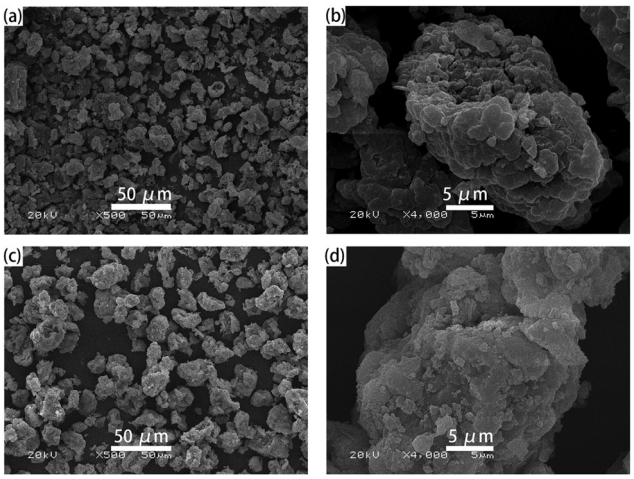

Fig. 1 (a and b) SEM images of IMI-P. (c and d) SEM images of ReO_4^- loaded IMI-P.

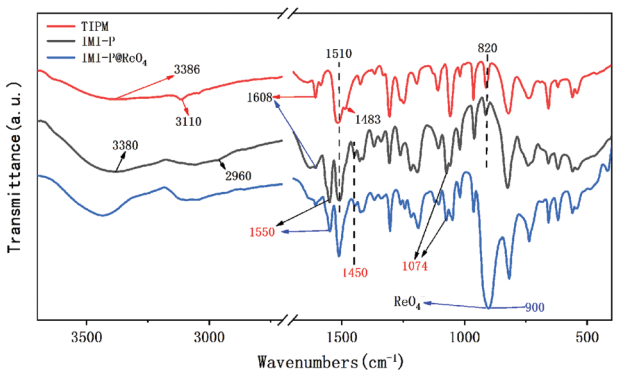

Fig. 2 FT-IR spectra of TIPM, IMI-P, and ReO_4^- loaded IMI-P.

Peaks at 3386 cm^{-1} and 3380 cm^{-1} are assigned to sorption water in TIPM and IMI-P, respectively.

The EDS spectra (Fig. 3a) and SEM elemental mapping (Fig. 3b) of IMI-P show a strong peak and the uniform distribution of the Cl element, respectively, indicating a homogeneous nature and high crosslinking degree of IMI-P. The chemical composition of IMI-P is further determined by XPS, and the peaks of C, N, O and Cl are shown in the full survey spectra (Fig. S1, ESI†). From the result of nitrogen adsorption–desorption at 77 K (Fig. S2, ESI†), negligible nitrogen capacity was adsorbed and the calculated BET surface area was about 2 m^2 g^{-1}. This low nitrogen adsorption capacity should be ascribed to plenty of anions existing in IMI-P, which blocked the nitrogen inside the material.

The adsorption kinetics

The imidazolium cationic networks were used to adsorb TcO_4^- in the aqueous phase. Because of the radioactivity of TcO_4^-, ReO_4^- was initially used as a nonradioactive structural analogue of $^{99}TcO_4^-$. As suggested in Fig. 4a, IMI-P removes 90% of ReO_4^- in 30 s and 99% ReO_4^- in 10 min, which is much faster than commercial materials.[27] During the first 30 s, the ReO_4^- concentration dropped to a very low level due to the high adsorption efficiency. The adsorption rate is related to the concentration of ReO_4^- and slows down after 30 s until equilibrium is reached. The experimental data are fitted with the PFO model, PSO model, and MO model. The PSO model fitted well with experimental data with correlation coefficient > 0.99. The MO model showed that k_1 is 0 min^{-1} and k_2 is 0.1221 g mg^{-1} min^{-1}, which further illustrated that the adsorption process follows the PSO model. The PSO model indicates that active sites are abundant in the adsorbent and the rate-controlling steps are related to the active sites rather than external and internal diffusion.[38]

At the time of 60 min, the distribution coefficient (K_d) of ReO_4^- reaches 1.3 × 10^5 mL g^{-1}, and that was a high value among various Re adsorption materials. The fast dynamics indicates that there are abundant pores in the designed three-dimensional framework. Another important reason for the fast kinetics should be attributed to the hydrophobicity of IMI-P caused by the presence of large numbers of phenyl groups. These two aspects together improve the mass transfer properties.

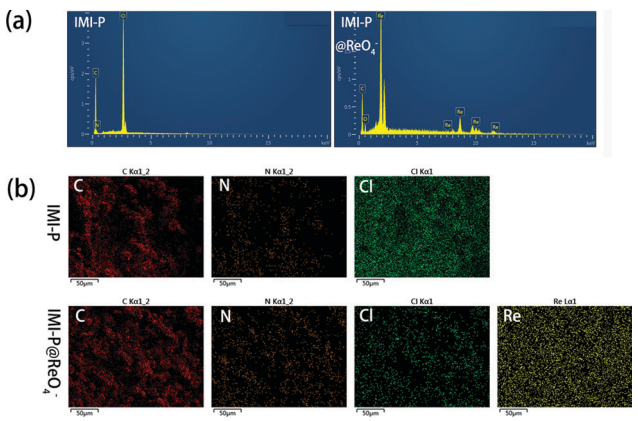

Fig. 3 (a) EDS spectra of ReO_4^- loaded MIM-P and MIM-P. (b) EDS mapping of MIM-P and ReO_4^- loaded MIM-P.

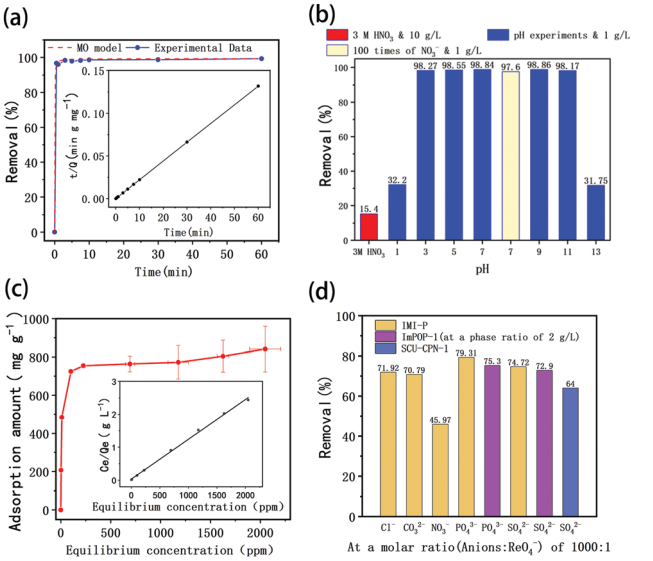

Fig. 4 (a) The ReO_4^- sorption kinetic curve and the inset is the fitting curve based on the pseudo-second-order model. (b) The removal efficiencies of ReO_4^- at different pH values and at 3 M HNO_3. (c) The ReO_4^- sorption isotherm curve, and the inset is the fitting curve based on the Langmuir model. (d) The removal efficiencies of ReO_4^- at the molar ratio of 1000 : 1.

pH effect

The effect of environmental pH on the adsorption of Tc by IMI-P was also studied. As shown in Fig. 4b, in a pH value range of 3–11, IMI-P has excellent adsorption performances, and can remove 98.1% of ReO_4^-. Like most imidazolium cationic frameworks, the adsorption performance for ReO_4^- is dramatically reduced under strong acid or alkali conditions.[27,33] When pH < 3 and pH > 11, the adsorption percentage drops sharply to 32.2% and 31.8%, respectively. In order to investigate whether the decrease in adsorption performance is caused by nitrate ion or hydrogen ion, the removal efficiencies at pH 1 (molar ratio of ReO_4^- : NO_3^- is 125 : 1) and at neutral conditions (100 : 1,Table 1) were compared. Even though the nitrate concentration in the two cases was similar, the removal efficiencies were quite different, and are 32.2% and 97.6%, respectively (Fig. 4b). It seems that hydrogen ions show a stronger effect for ReO_4^- adsorption. As shown in Fig. 4b, when the concentration of nitric acid is 3 M (the molar ratio of NO_3^- to ReO_4^- is about 2300 : 1, and the solid–liquid ratio is 10 g L^{-1}), the removal efficiency of ReO_4^- is reduced to 15.4%. After soaking IMI-P in 3 M nitric acid for 24 hours, it still maintained a similar adsorption capacity to the unsoaked material. This shows that this material is quite stable in acidic solution. For trace concentration of Tc (7.31 ppb) in 3 M nitric acid, 30.5% was removed at the solid–liquid ratio of 5 g L^{-1}. This indicates

Table 1 Adsorption performance of IMI-P with the coexistence of competing anions and ReO_4^-

Compounds	Concentration of compounds (M)	Molar ratio of coexisting anions to Re	Adsorption percentage (%)	K_d (mL g^{-1})
K_2SO_4	1.5×10^{-2}	100	95.0	1.9×10^4
K_2SO_4	1.5×10^{-1}	1000	74.7	3.0×10^3
$NaNO_3$	1.5×10^{-2}	100	97.6	4.1×10^4
$NaNO_3$	1.5×10^{-1}	1000	45.9	8.5×10^2
Na_2CO_3	1.5×10^{-2}	100	96.4	2.7×10^4
Na_2CO_3	1.5×10^{-1}	1000	70.7	2.4×10^3
K_3PO_4	1.5×10^{-2}	100	95.8	2.3×10^4
K_3PO_4	1.5×10^{-1}	1000	79.3	3.8×10^3
NaCl	1.5×10^{-1}	1000	71.9	2.6×10^3
K_2SO_4[a]	$7.38 \times \times 10^{-5}$	1000	99.3	1.45×10^5

[a] TcO_4^- aqueous solution (7.38×10^{-8} M) coexists with SO_4^{2-} at 1000 times the TcO_4^- concentration.

that IMI-P exhibits a good adsorption performance for TcO_4^- under such harsh conditions (NO_3^- in 4×10^7 times excess).

When pH > 13, it can be observed that the colour of IMI-P changed from white to yellow, indicating that the imidazolium cationic framework is decomposed under high alkalinity. The C2 proton of the imidazole ring is weakly acidic, which will lead to ring-opening reaction in the presence of a strong base.[39]

Adsorption isotherms

The adsorption isothermal model of IMI-P for Re was also evaluated and the experimental data was fitted with the Langmuir model. It fitted well with the correlation coefficient R^2 = 0.98 (Fig. 4c). This shows that the adsorption is monolayer, and the adsorption sites are uniform. The maximum sorption capacity of IMI-P calculated based on the Langmuir model is 792 mg ReO_4^- g^{-1}, close to the experimental value, which is an outstanding capacity larger than those of commercial materials such as Purolite A532E (446 mg g^{-1}) and A530E (706 mg g^{-1}).[27] The abundant imidazolium cationic sites are the key to high capacity, and the high affinity of imidazolium for ReO_4^- derives from the combination of Coulomb force and coordination. Purolite A530E and Purolite A532E contain a large number of ammonium active sites that bind ReO_4^- only by Coulomb forces and have lower capacity than IMI-P. Compared with the non-ionic adsorbent NU-2000, which binds ReO_4^- only by coordination, the capacity is 210 mg g^{-1}, which is lower than most anion exchange materials.[40]

However, the maximum sorption capacity is lower than the theoretic sorption capacity of 1070 mg g^{-1} (calculated with the mass of material) indicating that a little chlorine is retained in the ReO_4^- loaded IMI-P. The main reason for the incomplete chlorine exchange is the large particle size of IMI-P and the presence of unreacted chloromethyl groups in IMI-P, which can also be seen from the EDS spectra and the EDS Cl element mapping (Fig. 3).

Selectivity experiments

Considering the coexistence of a large number of anions with TcO_4^- in nuclear industrial wastewater, the effect of coexisting anions with different charges on adsorption of ReO_4^- was also investigated. From experimental results shown in Table 1 and Fig. 4d, when the molar ratio of Cl^-, CO_3^{2-}, NO_3^-, PO_4^{3-}, or SO_4^{2-} to ReO_4^- is 100 : 1, the removal percentages of ReO_4^- exceed 95%. At a molar ratio of 1000 : 1, the order of the influence of coexisting anions on ReO_4^- adsorption is $NO_3^- > Cl^- \approx CO_3^{2-} > SO_4^{2-} > PO_4^{3-}$. That is, the order of selectivity of IMI-P to anions is $ReO_4^- \gg NO_3^- > Cl^- \approx CO_3^{2-} > SO_4^{2-} > PO_4^{3-}$, which basically follows the Hofmeister order. The Hofmeister behavior in anion partitioning corresponds to adsorption strength increase with anion hydration Gibbs energy decrease. Anions with high charge density have high hydrated Gibbs energy and low affinity for hydrophobic materials, while anions with low charge density, such as NO_3^- and ReO_4^-, have low hydrated Gibbs energy and high affinity for hydrophobic materials.[41] This sequence is in conflict with the extent of electrostatic interaction between imidazolium and anions, suggesting that the electrostatic interaction does not play a major role in this case. In fact, in addition to the electrostatic interaction in the anion exchange process, the influence of the properties of the material itself on the affinity of the anion must also be considered. IMI-P is a hydrophobic material with a strong affinity for low charge density anions such as TcO_4^-/ReO_4^- and NO_3^-. At the same time, it is rich in imidazolium and has a specific interaction with TcO_4^-/ReO_4^-, so its affinity for TcO_4^-/ReO_4^- is higher than that for NO_3^-, resulting in higher selectivity for TcO_4^-/ReO_4^- than for NO_3^-.

As can be seen from Table 1, IMI-P has good adsorption capacity and selectivity for TcO_4^-/ReO_4^-. For instance, when coexistence PO_4^{3-} excess 1000 times of ReO_4^-, Re remove efficiency was 79.3%, higher than that of ImPOP-1 (75.3%).[33] When SO_4^{2-} was 1000 times in excess, the Re removal efficiency was 74.7%, higher than that of SCU-CPN-1 (64%) and ImPOP-1 (72.9%).[27,33] When trace amounts of TcO_4^- and SO_4^{2-} at more than 1000 times the concentration of TcO_4^- coexist, the Tc removal efficiency is 99.3%, and its concentration is reduced from 7.31 ppb to 0.05 ppb. The good selectivity for TcO_4^- and the excellent performance in removing trace amounts of TcO_4^- indicate that IMI-P has the potential to remediate TcO_4^--contaminated water bodies.

Although ReO_4^- behaves similarly to TcO_4^- in water, there are some differences in their affinity for the material based on the adsorption data above. For insight into the adsorption performance of IMI-P for Tc/Re under actual conditions, simulated wastewater was prepared by the reported method.[27] The composition of the simulated wastewater is shown in Table 2, NO_3^-, NO_2^- and Cl^- as the main competing anions coexist with ReO_4^-/TcO_4^- in the simulated wastewater, and the amount of these anions is more than 300 times that of ReO_4^-/TcO_4^-.

For the simulated Re-containing solution, when the solid-to-liquid ratio is 1 g L^{-1} and 10 g L^{-1}, the removal percentages of ReO_4^- are 36.5% and 85.8%, respectively. For the simulated Tc-containing solution, the adsorption percentage under different solid–liquid ratios is shown in Fig. 5a. The removal efficiencies increase with the increase of the solid–liquid ratios, and the K_d also increases with the increase of the solid–liquid ratios (in the

Table 2 Composition of the simulated wastewater

Anions	Concentration (M)	Molar ratio of anions to ReO_4^-
TcO_4^-/ReO_4^-	1.94×10^{-4}	1
NO_3^-	6.07×10^{-2}	314
Cl^-	6.39×10^{-2}	330
NO_2^-	1.69×10^{-1}	873
SO_4^{2-}	6.64×10^{-6}	0.0343
CO_3^{2-}	4.30×10^{-5}	0.222

inset curve) eventually reaching about 1350 mL g^{-1}. Compared with the results of simulated wastewater containing Re, the removal efficiencies of simulated wastewater containing Tc were higher, exceeding 90.1% at 10 g L^{-1} (for Re, 85.8%) and finally reaching 98.4% at 50 g L^{-1}. Therefore, this shows that IMI-P exhibits a better affinity for TcO_4^-. The reason for this result is that TcO_4^- is softer than ReO_4^- and is more easily embedded in the lipophilic backbone of IMI-P. The adsorption performance of IMI-P for TcO_4^- in simulated wastewater is similar to that of SCU-100 (87% at 5 g L^{-1}) and PQA-*p*NH_2Py-Cl (87.8% at 5 g L^{-1}), but slightly lower than that of PQA-*p*$N(Me)_2$Py-Cl (94.6% at 5 g L^{-1}) and PQA-Py-Cl (92.6% at 5 g L^{-1}).[31,42]

In order to investigate the influence of the main competing anions in the simulated waste liquid on the Tc adsorption, we performed the adsorption experiments of Tc by IMI-P simultaneously in the absence of coexisting anions and in the presence of coexisting anions at more than 1000 times the concentration of Tc. As shown in Fig. 5b, when the solid–liquid ratio is 5 g L^{-1}, without competing anions, IMI-P can remove more than 99.6% of TcO_4^-. When the concentrations of NO_3^-, NO_2^-, and Cl^- exceed 1000 times that of TcO_4^-, the Tc removal efficiencies are 84.1%, 91.8% and 93.8% respectively. Combining the results of selectivity experiments, the affinity of IMI-P to anions follows the order, $TcO_4^- > ReO_4^- \gg NO_3^- > NO_2^- > Cl^- \approx CO_3^{2-} > SO_4^{2-} > PO_4^{3-}$. The affinity of IMI-P to ReO_4^-/TcO_4^- far exceeds that of other anions. This extraordinary affinity may be due to the specific interaction between the ReO_4^-/TcO_4^- tetrahedron and the imidazolium ring. The imidazolium ring has been proved to have strong p–π interactions with single-charged tetrahedral anions such as ReO_4^- and MnO_4^-.[24] Spatial configuration is one of the important factors for the formation of strong interactions. One side of tetrahedral TcO_4^- parallel to the imidazolium rings forms a face-to-face stacking interaction while the one vertex of triangular NO_3^- close to imidazolium forms a corner-to-corner interaction.[27] Therefore, the selectivity of IMI-P with a large amount of imidazolium rings to TcO_4^- is much greater than that for NO_3^-. The interaction between IMI-P and TcO_4^- will be confirmed by subsequent XPS experiments.

Compared with other materials, the easier synthesis procedure, similar kinetics but larger particle size, better selectivity, and the ability to remove TcO_4^- from a complex environment indicate that IMI-P has a greater potential for industrial application.

The adsorption mechanism

In order to investigate the adsorption process, the ReO_4^- loaded IMI-P was characterized by FTIR, SEM, EDS, and XPS. Compared to the FTIR spectra of IMI-P (Fig. 2), the FTIR spectrum of IMI-P@ReO_4^- shows the appearance of a peak at 900 cm^{-1} which is assigned to the Re–O v_3 asymmetric stretching.[33] From SEM images (Fig. 1c and d), the morphology and size are unchanged, which indicates that IMI-P possesses high stability during adsorption progress. EDS images and element mapping (Fig. 3) show a sharp decrease in Cl content, and the appearance of a large amount of Re element indicates that the Cl element is replaced by the Re element, while the distribution of C and N elements is almost unchanged. These results demonstrate that the mechanism of the adsorption is anion exchange between Cl^- and ReO_4^-. The specific interaction between ReO_4^- and IMI-P was verified by X-ray photoelectron spectroscopy (XPS) (Fig. 6). The energy scales of the XPS spectra were calibrated using the C 1s peak at 284.8 eV. From the full survey spectra before and after adsorption (Fig. S1, ESI†), the disappearance of the peak of Cl (198 eV) and the appearance of the peak of Re (45 eV) further proved the mechanism of anion exchange. In the N 1s spectra, 400.98 eV and 401.12eV are the binding energies of imidazolium N 1s before and after adsorption, with a shift of 0.14 eV, indicating the decrease of electron density of N, and 398.75 eV and 398.77 eV are the binding energies of uncross-linked imidazole N 1s, and there is almost no change before and after adsorption. The analysis of the binding energy of N from imidazolium and imidazole further suggests that the ReO_4^- adsorption is driven by electrostatic interaction and is promoted by further interaction with the active site of the imidazolium ring. The binding energy of O 1s in perrhenate, after adsorption, shifts

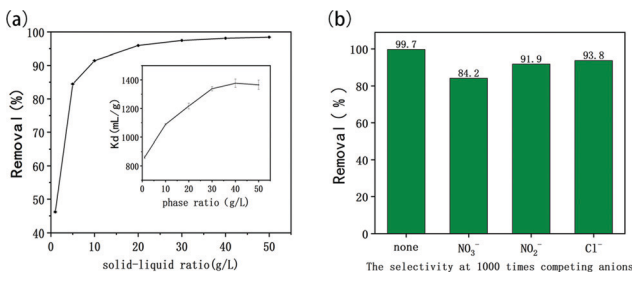

Fig. 5 (a) The removal percentages of Tc in simulated wastewater at various solid–liquid ratios, and the inset curve is K_d (mL g^{-1}) value at various solid–liquid ratios. (b) The removal efficiencies of Tc in the presence of 1000-fold excess anions.

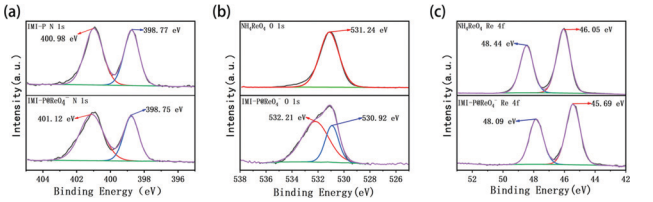

Fig. 6 The XPS analysis of (a) N 1s survey of IMI-P and ReO_4^- loaded IMI-P. (b) O 1s survey of NH_4ReO_4 and ReO_4^- loaded IMI-P. (c) Re 4f survey of NH_4ReO_4 and ReO_4^- loaded IMI-P.

0.97 eV from 531.24 eV (NH_4ReO_4) to 532.21 eV (IMI-P@ReO_4^-) indicating that the electron density of O atoms decreased, and the peak at 530.92 eV with smaller area belongs to the binding energy of O 1s in oxygen-containing impurities. From the Re 4f spectra, Re species retain the oxidation state of Re(VII), existing in the form of ReO_4^-. The peak of $4f_{5/2}$ shows a −0.35 eV shift from 48.44 eV (NH_4ReO_4) to 48.09 eV (IMI-P@ReO_4^-), and the peak of $4f_{7/2}$ shows a −0.36 eV shift from 46.05 eV (NH_4ReO_4) to 45.69 eV (IMI-P@ReO_4^-), indicating an increase in electron density. The change in the binding energy of N of imidazolium cations, and O and Re of perrhenate is caused by the strong interaction between the imidazolium cation and the ReO_4^- anion, which bestows on IMI-P high adsorption capacity and excellent selectivity. This result also suggests that the imidazolium group is a key region for preparing the adsorbent for ReO_4^-/TcO_4^- removal.

Desorption

ReO_4^- loaded IMI-P was eluted by 1 M NaCl solution, 47% desorbed at room temperature and 85% desorbed at 80 °C. If desorbed with saturated sodium chloride solution, the desorption efficiency is 58% at room temperature. The high temperature required for complete desorption also indicates a strong interaction between IMI-P and TcO_4^-/ReO_4^-.

Conclusions

In this contribution, a one-pot synthesis strategy for constructing a three-dimensional network using tetrahedral imidazolylphenylmethane and polyhalogenated benzene is demonstrated. The advantages of this material in separating Tc lie in its high extraction capacity, good selectivity, fast kinetics and larger particle size which facilitates column chromatography for TcO_4^- removal from nuclear industrial wastewater. These excellent properties are determined by its structure. The hydrophobic framework and three-dimensional structure of the material improve its fast mass transfer properties. The high-density imidazolium cation in the framework provides both a positive charge and an active site that can interact with TcO_4^- which makes it have high adsorption capacity and selectivity for TcO_4^- anions. XPS and EDS proved that the adsorption process was anion exchange, and TcO_4^- with stronger affinity for the material entered into the adsorbent and replaced Cl^- as a counter ion. The adsorption process is driven by electrostatic interaction and is promoted by further interaction with the active site of the imidazolium ring. In the simulated wastewater environment, IMI-P shows good performance in removing TcO_4^- at pH 3–11, so IMI-P has important potential applications in nuclear industry wastewater treatment and the remediation of Tc-containing environments. IMI-P is stable in 3 M HNO_3 aqueous solution and has considerable adsorption performance, and can be used for the treatment of high-level liquid waste. This strategy not only develops a material with strong anion exchange capacity but also improves the mass transfer properties that may lead to more efficient separation.

Conflicts of interest

There are no conflicts to declare.

Acknowledgements

This work was supported by the National Natural Science Foundation of China (21976075).

Notes and references

1 World Energy Outlook 2021 – Analysis - IEA, https://www.iea.org/reports/world-energy-outlook-2021).
2 R. Taylor, *Chemistry*, 2016, **1**, 662.
3 S. J. Yu, H. Tang, D. Zhang, S. Q. Wang, M. Q. Qiu, G. Song, D. Fu, B. W. Hu and X. K. Wang, *Sci. Total Environ*, 2022, **811**, 19.
4 In *The Future of Nuclear Power*, ed. J. N. Lillington, Elsevier Ltd, 2004.
5 K. Yoshihara, in *Technetium and Rhenium: Their Chemistry and Its Applications*, ed. K. Yoshihara and T. Omori, Springer-Verlag; Berlin, Berlin, 1996, vol. 176, pp. 17–35.
6 B. C. Childs, F. Poineau, K. R. Czerwinski and A. P. Sattelberger, *J. Radioanal. Nucl. Chem.*, 2015, **306**, 417–421.
7 J. G. Darab and P. A. Smith, *Chem. Mater.*, 1996, **8**, 1004–1021.
8 In *The analytical chemistry of technetium*, ed. K. Schwochau, Springer, Berlin, Heidelberg, 1981.
9 J. P. Icenhower, N. P. Qafoku, J. M. Zachara and W. J. Martin, *Am. J. Sci.*, 2010, **310**, 721–752.
10 C. I. Pearce, R. J. Serne, S. A. Saslow, W. Um, R. M. Asmussen, M. D. Miller, O. Qafoku, M. M.-V. Snyder, C. T. Resch, K. C. Johnson, G. H. Wang, S. M. Heald, J. E. Szecsody, J. M. Zachara, N. P. Qafoku, A. E. Plymale and V. L. Freedman, *ACS Earth Space Chem.*, 2018, **2**, 1145–1160.
11 H. Deng, Z. J. Li, X. C. Wang, L. Wang, K. Liu, L. Y. Yuan, Z. Y. Chang, J. K. Gibson, L. R. Zheng, Z. F. Chai and W. Q. Shi, *Environ. Sci. Technol.*, 2019, **53**, 10917–10925.
12 T. Peretyazhko, J. M. Zachara, S. M. Heald, R. K. Kukkadapu, C. Liu, A. E. Plymale and C. T. Resch, *Environ. Sci. Technol.*, 2008, **42**, 5499–5506.
13 S. M. Qaim, *J. Inorg. Nucl. Chem.*, 1966, **28**, 666–668.
14 J. Li, L. Zhu, C. L. Xiao, L. H. Chen, Z. F. Chai and S. A. Wang, *Radiochim. Acta*, 2018, **106**, 581–591.
15 K. H. Goh, T. T. Lim and Z. Dong, *Water Res.*, 2008, **42**, 1343–1368.
16 L. Zhu, L. J. Zhang, J. Li, D. Zhang, L. H. Chen, D. P. Sheng, S. T. Yang, C. L. Xiao, J. Q. Wang, Z. F. Chai, T. E. Albrecht-Schmitt and S. Wang, *Environ. Sci. Technol.*, 2017, **51**, 8606–8615.
17 S. A. Wang, E. V. Alekseev, D. W. Juan, W. H. Casey, B. L. Phillips, W. Depmeier and T. E. Albrecht-Schmitt, *Angew. Chem., Int. Ed.*, 2010, **49**, 1057–1060.
18 F. F. Dong, X. M. Li, Y. W. Huang, X. P. Zhi, S. L. Yang and Y. L. Shen, *ACS Omega*, 2021, **6**, 25672–25679.

19 S. Dutta, P. Samanta, B. Joarder, S. Let, D. Mahato, R. Babarao and S. K. Ghosh, *ACS Appl. Mater. Interfaces*, 2020, **12**, 41810–41818.
20 I. R. Colinas, R. C. Silva and S. R.-J. Oliver, *Environ. Sci. Technol.*, 2016, **50**, 1949–1954.
21 N. N. Shen, Z. X. Yang, S. T. Liu, X. Dai, C. L. Xiao, K. Taylor-Pashow, D. E. Li, C. Yang, J. Li, Y. G. Zhang, M. X. Zhang, R. H. Zhou, Z. F. Chai and S. Wang, *Nat. Commun.*, 2020, **11**, 12.
22 S. J. Yu, H. W. Pang, S. Y. Huang, H. Tang, S. Q. Wang, M. Q. Qiu, Z. S. Chen, H. Yang, G. Song, D. Fu, B. W. Hu and X. X. Wang, *Sci. Total Environ.*, 2021, **800**, 22.
23 L. Zhu, D. P. Sheng, C. Xu, X. Dai, M. A. Silver, J. Li, P. Li, Y. X. Wang, Y. L. Wang, L. H. Chen, C. L. Xiao, J. Chen, R. H. Zhou, C. Zhang, O. K. Farha, Z. F. Chai, T. E. Albrecht-Schmitt and S. Wang, *J. Am. Chem. Soc.*, 2017, **139**, 14873–14876.
24 S. S. Jiao, L. M. Deng, X. H. Zhang, Y. W. Zhang, K. Liu, S. X. Li, L. Wang and D. X. Ma, *ACS Appl. Mater. Interfaces*, 2021, **13**, 39404–39413.
25 J. Li, B. Y. Li, N. N. Shen, L. X. Chen, Q. Guo, L. Chen, L. W. He, X. Dai, Z. F. Chai and S. Wang, *ACS Cent. Sci.*, 2021, **7**, 1441–1450.
26 Y. W. Xu, Y. Tian, B. Chen, Z. J. Yan, J. Ding, Y. L. Huang, J. Y. Kang, S. Y. Chen, Y. D. Jin and C. Q. Xia, *J. Radioanal. Nucl. Chem.*, 2021, **330**, 1165–1176.
27 J. Li, X. Dai, L. Zhu, C. Xu, D. Zhang, M. A. Silver, P. Li, L. H. Chen, Y. Z. Li, D. W. Zuo, H. Zhang, C. L. Xiao, J. Chen, J. Diwu, O. K. Farha, T. E. Albrecht-Schmitt, Z. F. Chai and S. A. Wang, *Nat. Commun.*, 2018, **9**, 3007.
28 M. Hao, Z. Chen, H. Yang, G. I.-N. Waterhouse, S. Ma and X. Wang, *Sci. Bull.*, 2022, **67**, 924–932.
29 J. Li, L. Chen, N. N. Shen, R. Z. Xie, M. V. Sheridan, X. J. Chen, D. P. Sheng, D. Zhang, Z. F. Chai and S. Wang, *Sci. China: Chem.*, 2021, **64**, 1251–1260.
30 K. M. Long, G. S. Goff, S. D. Ware, G. D. Jarvinen and W. H. Runde, *Ind. Eng. Chem. Res.*, 2012, **51**, 10445–10450.
31 Q. Sun, L. Zhu, B. Aguila, P. K. Thallapally, C. Xu, J. Chen, S. Wang, D. Rogers and S. Q. Ma, *Nat. Commun.*, 2019, **10**, 9.
32 Y. Wang, D. Han, S. C. Zhong, X. X. Li, H. Su, T. W. Chu, J. Peng, L. Zhao, J. Q. Li and M. L. Zhai, *J. Hazard. Mater.*, 2021, **401**, 9.
33 Z. W. Liu and B. H. Han, *Environ. Sci. Technol.*, 2020, **54**, 216–224.
34 X. Li, Y. Li, H. Wang, Z. Niu, Y. He, L. Jin, M. Wu, H. Wang, L. Chai, A. M. Al-Enizi, A. Nafady, S. F. Shaikh and S. Ma, *Small*, 2021, **17**, 2007994.
35 B. Y. Li, Q. Sun, Y. M. Zhang, C. W. Abney, B. Aguila, W. B. Lin and S. Q. Ma, *ACS Appl. Mater. Interfaces*, 2017, **9**, 12511–12517.
36 R. Custelcean and B. A. Moyer, *Eur. J. Inorg. Chem.*, 2007, 1321–1340, DOI: **10.1002/ejic.200700018**.
37 X. Guo and J. L. Wang, *J. Mol. Liq.*, 2019, **288**, 8.
38 J. L. Wang and X. Guo, *J. Hazard. Mater.*, 2020, **390**, 18.
39 B. S. Wang, L. Qin, T. C. Mu, Z. M. Xue and G. H. Gao, *Chem. Rev.*, 2017, **117**, 7113–7131.
40 R. J. Drout, K. Otake, A. J. Howarth, T. Islamoglu, L. Zhu, C. L. Xiao, S. Wang and O. K. Farha, *Chem. Mater.*, 2018, **30**, 1277–1284.
41 L. Escobar and P. Ballester, *Chem. Rev.*, 2021, **121**, 2445–2514.
42 D. P. Sheng, L. Zhu, C. Xu, C. L. Xiao, Y. L. Wang, Y. X. Wang, L. H. Chen, J. Diwu, J. Chen, Z. F. Chai, T. E. Albrecht-Schmitt and S. A. Wang, *Environ. Sci. Technol.*, 2017, **51**, 3471–3479.